BIOCHEMISTRY
including biophysical chemistry & molecular biology

Article

pubs.acs.org/biochemistry

Local Destabilization of the Metal-Binding Region in Human Copper−Zinc Superoxide Dismutase by Remote Mutations Is a Possible Determinant for Progression of ALS

Janosch Hennig,[†,‡,§] Cecilia Andrésen,[†] A. Katrine Museth,[†,⊥] Patrik Lundström,[†] Lena A. E. Tibell,[∥] and Bengt-Harald Jonsson*[,†]

[†]Division of Molecular Biotechnology, Department of Physics, Chemistry and Biology, Linköping University, SE-581 83, Linköping, Sweden

[‡]Institute of Structural Biology, Helmholtz Zentrum München GmbH, DE-85764 Neuherberg, Germany

[§]Chair of Biomolecular NMR Spectroscopy, Department of Chemistry, Technische Universität München, DE-85748 Garching, Germany

[∥]Department of Science and Technology, Linköping University, SE-601 74, Norrköping, Sweden

[⊥]Division of Chemistry and Chemical Engineering, California Institute of Technology, Pasadena, California 91125, United States

Supporting Information

ABSTRACT: More than 100 distinct mutations in the gene *CuZnSOD* encoding human copper−zinc superoxide dismutase (CuZnSOD) have been associated with familial amyotrophic lateral sclerosis (fALS), a fatal neuronal disease. Many studies of different mutant proteins have found effects on protein stability, catalytic activity, and metal binding, but without a common pattern. Notably, these studies were often performed under conditions far from physiological. Here, we have used experimental conditions of pH 7 and 37 °C and at an ionic strength of 0.2 M to mimic physiological conditions as close as possible in a sample of pure protein. Thus, by using NMR spectroscopy, we have analyzed amide hydrogen exchange of the fALS-associated I113T CuZnSOD variant in its fully metalated state, both at 25 and 37 °C, where ^{15}N relaxation data, as expected, reveals that CuZnSOD I113T exists as a dimer under these conditions. The local dynamics at 82% of all residues have been analyzed in detail. When compared to the wild-type protein, it was found that I113T CuZnSOD is particularly destabilized locally at the ion binding sites of loop 4, the zinc binding loop, which results in frequent exposure of the aggregation prone outer β-strands I and VI of the β-barrel, possibly enabling fibril or aggregate formation. A similar study (Museth, A. K., et al. (2009) *Biochemistry*, *48*, 8817−8829) of amide hydrogen exchange at pH 7 and 25 °C on the G93A variant also revealed a selective destabilization of the zinc binding loop. Thus, a possible scenario in ALS is that elevated local dynamics at the metal binding region can result in toxic species from formation of new interactions at local β-strands.

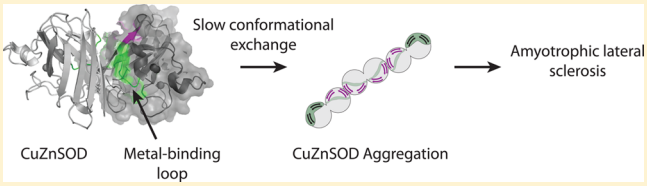

Amyotrophic lateral sclerosis (ALS) is a neurodegenerative disease that is characterized, as other diseases like Alzheimer's, Parkinson's, and Huntington's, by mid-to-late-life onset, selective neuronal death, and the formation of protein deposits in affected neuronal tissues.[1] The median age onset for ALS is at 46 years (range of 24−72 years), and the median duration of disease of 3 years (range of 0.3−20 years).[2] The affected neurologic tissues are the motor cortex, brain stem, and spinal cord.[3] Although most cases of ALS are sporadic, there is a genetic link, and familial ALS (fALS) has been found in roughly 10% of all reported cases of the disease. Approximately one in five cases has been directly attributed to autosomal dominant mutations in the *CuZnSOD* gene, which encodes the intracellular copper−zinc superoxide dismutase (CuZnSOD).[4−6] More than 100 distinct CuZnSOD mutations have been identified in fALS patients.[7] Interestingly, mutations are found throughout the gene and have been identified at more than one-third of the 153 amino acid positions in the wild-type CuZnSOD protein; yet, in most instances, these mutations do not significantly lower the CuZnSOD activity of the resulting enzyme,[8] and how these mutations affect CuZnSOD and trigger disease is currently not known. However, transgenic mice expressing fALS mutant G93A developed progressive motor neuron disease, although high CuZnSOD activity was maintained.[9] Thus, CuZnSOD activity does not seem to be relevant for the development of disease, especially since transgenic mice with no endogenous CuZnSOD were found not to develop motor neuron disease.[10] One model for how the neurodegenerating toxicity in ALS arises is the formation of toxic aggregates.[11−14] Possibly structural destabilization, metal depletion, reduction of disulfide bonds, and/or change in the

Received: May 19, 2014
Revised: December 14, 2014
Published: December 15, 2014

ACS Publications © 2014 American Chemical Society

DOI: 10.1021/bi500606j
Biochemistry 2015, 54, 323−333

dynamic properties of CuZnSOD mutants may play a role in the formation of toxic aggregates and in the pathology of fALS.[14−21]

Human CuZnSOD is a homodimeric protein with a total mass of 32 kDa, containing one copper and one zinc ion per subunit. The copper ion mediates the disproportionation of a superoxide anion to hydrogen peroxide and dioxygen ($2O_2^- + 2H^+ \rightarrow O_2 + H_2O_2$) in a reduction−oxidation cycle between Cu(I) and Cu(II).[22] CuZnSOD is a crucial protein for the defense against superoxide anion radicals.[23] Therefore, CuZnSOD is expressed abundantly and makes up 1−2% of the total protein content in the cell. The determination of the high-resolution structure revealed that CuZnSOD adopts a Greek key β-barrel with one intramolecular disulfide bridge in each subunit.[24−26] This contributes to the high stability of the protein against thermal denaturation, detergents, and proteolysis.[27] Previous studies were hampered by expression systems that made only low-level metalation possible and led to serious problems in the production of active CuZnSOD variants. On the basis of the discovery of the network of copper-trafficking genes required for the incorporation of copper into proteins *in vivo*,[28,29] this problem was overcome by using a system for coexpression of CuZnSOD and the copper chaperone from yeast (yCCS), resulting in CuZnSOD variants with full copper ion content, which is a prerequisite condition for this study.[30] A possible reason for the need of a Cu-chaperone is that the Cu^{2+} ion has three side chain ligands situated in the rigid β-strands IV and VII and therefore efficient insertion might require chaperone-guided interactions at an early, more dynamical phase of the folding process.

Previous biophysical studies of ALS-associated CuZnSOD variants have been performed under varying conditions and show that different variants differ in characteristics such as melting temperature, Cu and Zn binding affinity, and net charge. Therefore, it has been suggested that CuZnSOD variants are likely to aggregate for different reasons.[31] Thus, structural changes attributed to the different mutations can be small and delicate and may escape detection upon analysis by X-ray crystallography and conventional biophysical methods. Also, earlier biophysical studies of the ALS-associated CuZnSOD variants have commonly been performed using pseudo-wild-type protein or variants with additional point mutations, and the environmental conditions have mostly been far from physiological.

In this study, we aim to gain understanding of the intrinsic dynamical and structural properties of the ALS-associated CuZnSOD variant I113T.[2,32] In *Drosophila*, it has been shown that flies with the I113T mutation have a significantly shorter lifetime than those with wild-type SOD.[33] Most importantly, we attempt to employ conditions that are as close as possible to the natural physiological conditions of the cell but that still allow measurements by high-resolution NMR methods to be made. Thus, we used 37 °C and pH 7 and an ionic strength of 0.2 M for all measurements, but we also repeated the measurements at 25 °C in order to compare and relate them to earlier studies. The results were then analyzed and compared with results from earlier similar studies, by us and others, of the wild-type protein and the G93A variant.[15,34,35] Taken together, these studies show that the metal binding region can be selectively destabilized by amino acid substitutions at remote positions. Several earlier studies on the structure of zinc-deficient SOD variants have also shown that increased flexibility at the zinc binding loop can induce nonnative interactions between subunits.[62−65] Thus, a possible scenario in ALS is that elevated local dynamics at the metal binding region can result in toxic species from formation of new interactions at local β-strands.

EXPERIMENTAL PROCEDURES

Expression and Purification of ^{15}N Human Intracellular CuZnSOD Mutant I113T. For this purpose, the pSOD1 plasmid with an additional insert of the gene encoding the yeast copper chaperone yCCS[29] was used and introduced into *Escherichia coli* strain Bl21(DE3). The use of this construct results in full copper incorporation in CuZnSOD.[30] The I113T mutation was constructed by use of the QuikChange kit from Agilent Technologies. The cells were grown at room temperature to an OD_{600} of 0.5−0.6 in minimal medium [Na_2HPO_4 (6 g/L), KH_2PO_4 (3 g/L), NaCl (0.5 g/L), glucose (10 g/L), $FeSO_4$ (0.01 mM), K_2SO_4 (0.28 mM), $CaCl_2$ (0.5 mM), $MgCl_2$ (1 mM), micrometernutrients excl. $CoCl_2$ (1 mL/L), vitamin mixture (1 mL/L), and $^{15}NH_4Cl$ (0.5 g/L)] containing 100 mg/L ampicillin. At the time of induction, 0.5 mM IPTG and $CuSO_4$ and $ZnSO_4$ were added to final concentrations of 0.1 and 1 mM, respectively. During the following 5 h, additional $CuSO_4$ at a concentration of 0.1 mM was added once an hour. Two hours before cells were harvested, additional $CuSO_4$ was added to a final concentration of 1 mM to ensure full and correct incorporation of copper ions. The cells were harvested by centrifugation (3600 rpm), resuspended in 20 mM potassium phosphate buffer (pH 7.0) containing DNase and RNase, and lysed by ultrasonication (Misonix). After centrifugation (14 900*g* for 45 min), ammonium sulfate (390 g/L supernatant) was added to the supernatant and stirred on ice for 2 h before further centrifugation (14 900*g* for 45 min). The supernatant was applied on a 50 mL phenyl sepharose 6 FF column (Amersham Biosciences) equilibrated with 2 M $(NH_4)_2SO_4$, 150 mM NaCl, and 50 mM KP_i (pH 7.0). The protein solution was washed with 150 mL before being eluted with 150 mM NaCl and 50 mM KP_i (pH 7.0) and a linear gradient from 2 to 0 M $(NH_4)_2SO_4$ in 300 mL. The protein eluted at 60%. The protein was further purified by gel filtration (Superdex 75, GE healthcare) using a buffer containing 20 mM KPi and 100 mM K_2SO_4, pH 7.0. Samples for H/D exchange experiments were further lyophilized.

NMR Spectroscopy of CuZnSOD I113T. All NMR measurements were carried out on a Varian Inova 600 MHz spectrometer equipped with a cryogenic probe head and a Varian Inova 800 MHz spectrometer equipped with a triple resonance room-temperature probe. All spectra were processed using NMRPipe.[36] Backbone assignments based on previous assignments[15] of wild-type CuZnSOD were confirmed by recording HNCA and CBCA(CO)NH[37] spectra that were analyzed by CARA (http://cara.nmr.ch). Peak volumes of all other experiments were fitted using the program PINT.[38]

Measurements and Analysis of ^{15}N Relaxation Data. Measurements of R_1, $R_{1\rho}$, and the ^{1}H−^{15}N heteronuclear NOE were performed at a static magnetic field corresponding to a proton Larmor frequency of 600 MHz at 25 and 37 °C using standard pulse sequences.[39,40] For the R_1 experiments, relaxation delays of 10*, 20, 50, 140, 180*, 240, 330, 410, 490, 560, 640, 650, 780, 910, 1000, 1130, and 1280* ms were employed at both temperatures. Duplicate data points for estimation of uncertainties in peak volumes were recorded for the relaxation delays and are indicated with an asterisk. The $R_{1\rho}$ experiments were recorded with spinlock fields of 1736 and 1678 Hz at 25 and 37 °C, respectively. Relaxation delays of 4*,

DOI: 10.1021/bi500606j
Biochemistry 2015, 54, 323−333

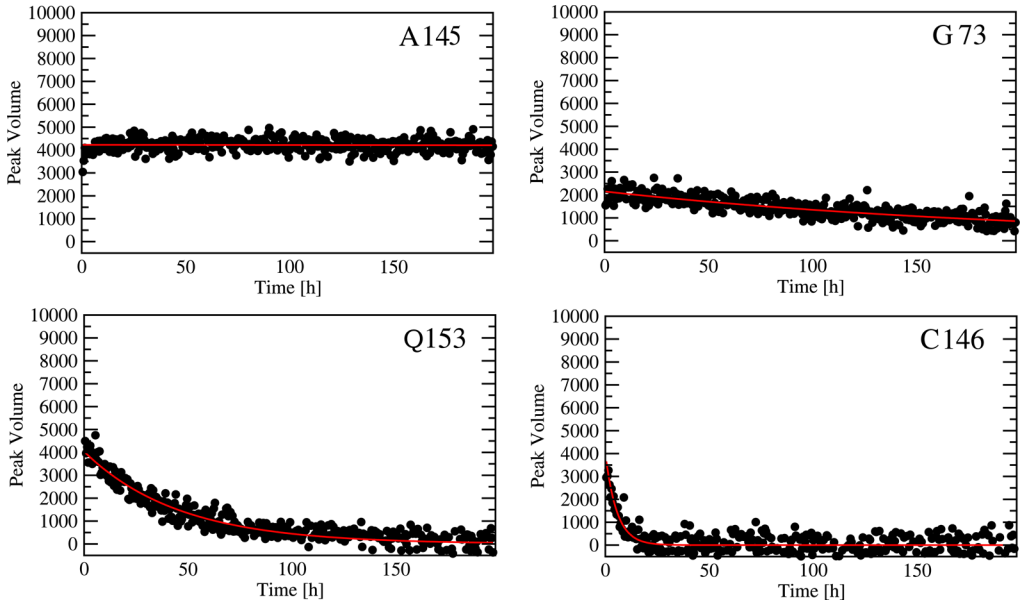

Figure 1. Representative plots for H/D exchange profiles for backbone amide protons for I113T at 37 °C. Residue alanine 145 shows no exchange during the time span measured (8 days). The other plots show residues with different H/D exchange rates (increasing from residue G73 over Q153 to C146).

6, 8, 10, 12, 16, 23, 26, 28, 36, 39, 42*, 46, and 50* ms were used in both cases. The heteronuclear NOE was calculated as the ratio of experiments including or excluding a 5 s period of proton saturation achieved by application of closely spaced 120° pulses. The total recovery delay was 12 s for both versions of the experiment.

Carr−Purcell−Meiboom−Gill (CPMG[41,42]) relaxation dispersion experiments at 25 °C were recorded at the same static field using a previously published pulse sequence.[43] Effective fields, defined as $\nu_{CPMG} = 1/(4\tau_{cp})$, where $2\tau_{cp}$ is the interval between successive refocusing pulses of 50*, 100*, 150, 200, 300, 400, 500*, 600, 700, 800*, 900, and 1000* Hz. Intensities were converted to effective transverse relaxation rates by the relation $R_{2,eff} = \ln(I_0)/I(\nu_{CPMG})/T$, where $I(\nu_{CPMG})$ is the intensity for different values of ν_{CPMG}, I_0 is the intensity obtained when the CPMG block is omitted, and T is the duration of the constant time relaxation delay (20 ms in this case). R_2 was calculated from $R_{1\rho}$ and R_1 as $R_2 = R_{1\rho}/\sin^2\theta - R_1/\tan^2\theta$, $\tan\theta = \nu_{sl}/\Omega$, where ν_{sl} is the spinlock field strength and Ω is the offset from the spinlock carrier frequency. The software TENSOR2[44] was used to estimate the diffusion tensor from the R_2/R_1 ratio. Residues with NOE < 0.65 were omitted from the analysis. The data was fitted to isotropic and anisotropic models, and F-tests were used to establish the appropriate model. The CPMG data was fitted to the Bloch−McConnell equations.[45] F-tests at a significance level of $p < 0.01$ were used to select between models including or excluding two-site chemical exchange.

Measurements of Rapid Amide Proton Exchange with Bulk Solvent. To measure exchange rates of rapidly exchanging (1.0 s^{-1}) backbone amide protons with solvent water at 25 and 37 °C, a 2D heteronuclear water exchange filter sequence (WEX II-FHSQC) was used.[46] As mixing times, 10, 30*, 50, 70, 80, 90*, 100, 110, 130, 150, and 170 ms were used. For the spin−echo WEX II-FHSQC, an echo time of 40 and 60 ms was used with mixing times of 10, 30, 40, 80, 110, 130, and 170 ms. The saturation factor was calculated to 0.54 and 0.64 at echo times 40 and 60 ms, respectively.[46] The measurements were performed at a Varian Inova 800 MHz spectrometer.

Sample Preparation, Measurements, and Data Analysis of H/D Exchange. The lyophilized protein, sodium isoascorbate, and a D_2O buffer (99% D_2O) containing 0.02 M potassium phosphate and 0.07 M K_2SO_4 (pH 7.0) were placed overnight in a glovebox under a nitrogen atmosphere to produce and maintain an anaerobic environment. The following day, the lyophilized protein sample was dissolved in 625 μL of D_2O buffer, of which 600 μL was transferred to the NMR tube. To reduce the Cu(II) ions to Cu(I), sodium iso-ascorbate was dissolved in D_2O buffer to a concentration 100 times greater than that of the protein (dimer), and 25 μL was added to the NMR tube, resulting in a 4-fold excess of the iso-ascorbate over protein. To observe H/D exchange, $^1H-^{15}N$ HSQC spectra were recorded consecutively over 3.5 and 8.4 days at 25 and 37 °C, respectively, using Varian Inova spectrometers (25 °C at 600 MHz and 37 °C at 800 MHz). The dead time before the first data point was recorded was 38 min (8 min for preparing the sample, tune the probe-head, shimming the magnet, and optimization of the 90° ^1H pulse; each spectrum ran for 30 min). All experiments at 800 MHz (37 °C) were acquired with 1536 data points in the direct dimension and 85 in the indirect dimension with eight scans and spectral widths of 12 001 (^1H) and 2600 (^{15}N) Hz. The parameters were scaled appropriately for the measurements at 600 MHz (25 °C). The amide hydrogen exchange rate, k_{ex}, at each residue was determined by fitting the measured time-dependent cross-peak volume to single-exponential decays, using the program PINT.[38] The corresponding ΔG values for the local unfolding were calculated as described in Bai et al.[47] Further details about the data evaluation can be obtained from Museth et al.[34]

RESULTS

Global Dynamics Assessed by ^{15}N Relaxation NMR. Relaxation experiments were used to investigate whether the molecule tumbles as a dimer or monomer in solution under near-physiological experimental conditions and if any higher

DOI: 10.1021/bi500606j
Biochemistry 2015, 54, 323−333

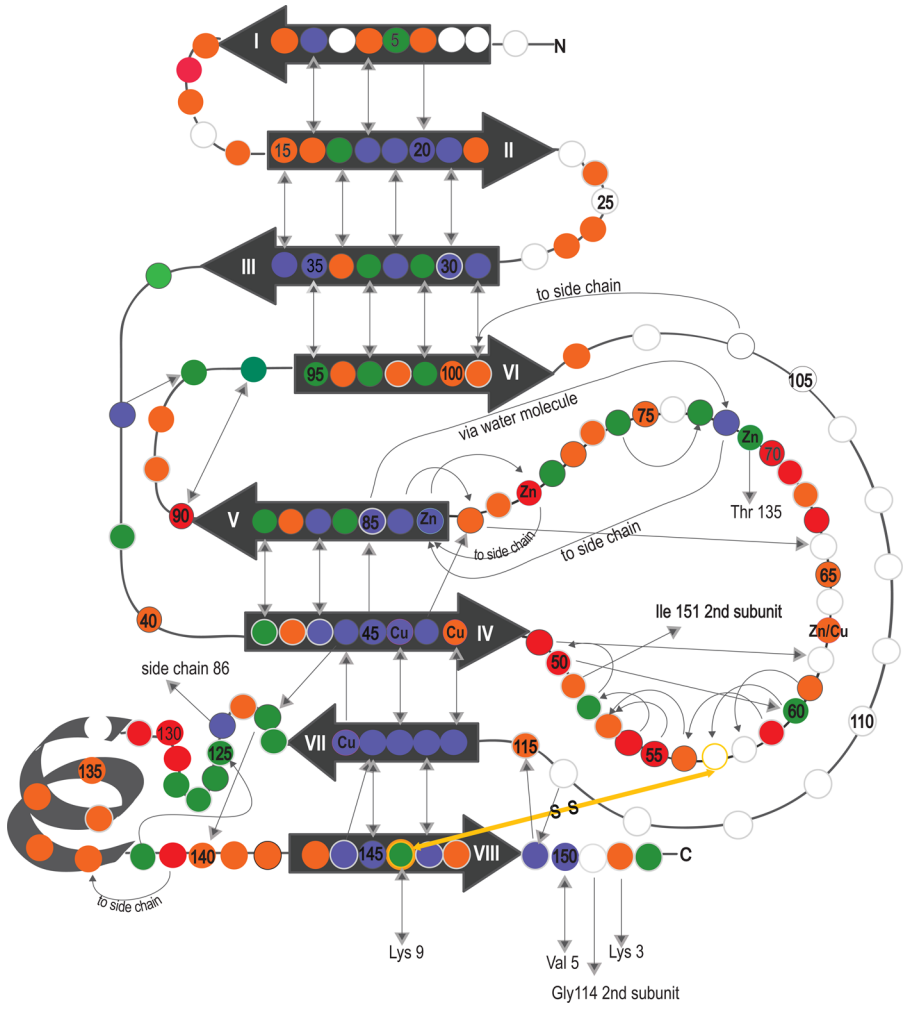

Figure 2. Schematic drawing of one CuZnSOD subunit showing the exchange pattern for the I113T variant at 37 °C. Amino acids for which the H/D exchange is too slow to be detected during the experimental time ($t_{1/2}$ longer than 13 days) are colored blue. Amide protons with quantifiable ($t_{1/2}$ 17 min to 13 days) exchange rates in the H/D exchange experiment are colored green. Amide protons, which were detected in the water exchange experiment and exchange with $t_{1/2}$ between 1 s and 17 min, are colored orange, and amide protons that exchange with $t_{1/2}$ between 10 ms and 1 s are colored red. Amino acids that are not assigned (prolines included) due to overlap and weak or missing peaks are colored white. Copper and zinc binding sites are labeled with Cu and Zn, respectively. The black numbered arrows illustrate the eight β-sheets, and the gray arrows between the amino acids indicate hydrogen bonds in the secondary structure, as determined from the crystal structure (PDB accession no. 2C9V) pointing from H to O.

order aggregates were present. A robust estimation of the correlation time for rotational diffusion of a protein is obtained from the R_2/R_1 ratio of residues in well-structured regions that do not experience chemical exchange broadening.[48] If the protein structure is also known, then all principal components of the diffusion tensor can be extracted for any rotational model. We used the program TENSOR2[44] together with a crystal structure of superoxide dismutase (PDB ID: 2C9V) to fit the data at the two temperatures. To exclude residues in unstructured regions, only those with NOE > 0.65 were considered. Results from CPMG experiments showed that no residues had to be excluded from the analysis because of millisecond dynamics. At both temperatures, the data were significantly better modeled by axially symmetric (prolate) rather than by isotropic rotation. A fully asymmetric model did not improve the fit significantly. Given the "cigar" shape of the superoxide dismutase dimer, this is the expected result. The three correlation times ($\tau_1 = 6D_\perp$, $\tau_2 = D_\parallel + 5D_\perp$, and $\tau_3 = 4D_\parallel + 2D_\perp$) for tumbling were τ_1 = 20.8 ns, τ_2 = 19.2 ns, and τ_3 = 15.6 ns at 25 °C and τ_1 = 14.9 ns, τ_2 = 13.9 ns, and τ_3 = 11.5 ns at 37 °C. These results indicate dynamics that are close to, but slightly faster than, previously published results on two other CuZnSOD variants studied at 25 °C.[15,35] Our results agree with the molecular tumbling time expected from calculation of the hydrodynamic properties[49] using the crystal structure of the wild-type CuZnSOD dimer (PDB ID: 2C9V), indicating that the I113T variant is indeed a stable dimer in solution and does not rapidly form higher order aggregates. Further support for this notion is that the experimental results were virtually identical when the experiments were repeated on the same sample that had been stored for 6 months at 4 °C. It is important to note that no residues exhibited conformational exchange in the millisecond time range.

H/D and Water Exchange in the I113T Variant at 37 °C. In order to assess the half-lives ($t_{1/2}$) for amide proton exchange in the interval between 10 ms and 1s, the exchange of amide protons with H_2O was measured by using magnetization transfer techniques.[46] For longer half-lives, hydrogen−deuterium exchange between amide protons and D_2O was measured with the usual setup of repetitive $^1H-^{15}N$ HSQC experiments

DOI: 10.1021/bi500606j
Biochemistry 2015, 54, 323−333

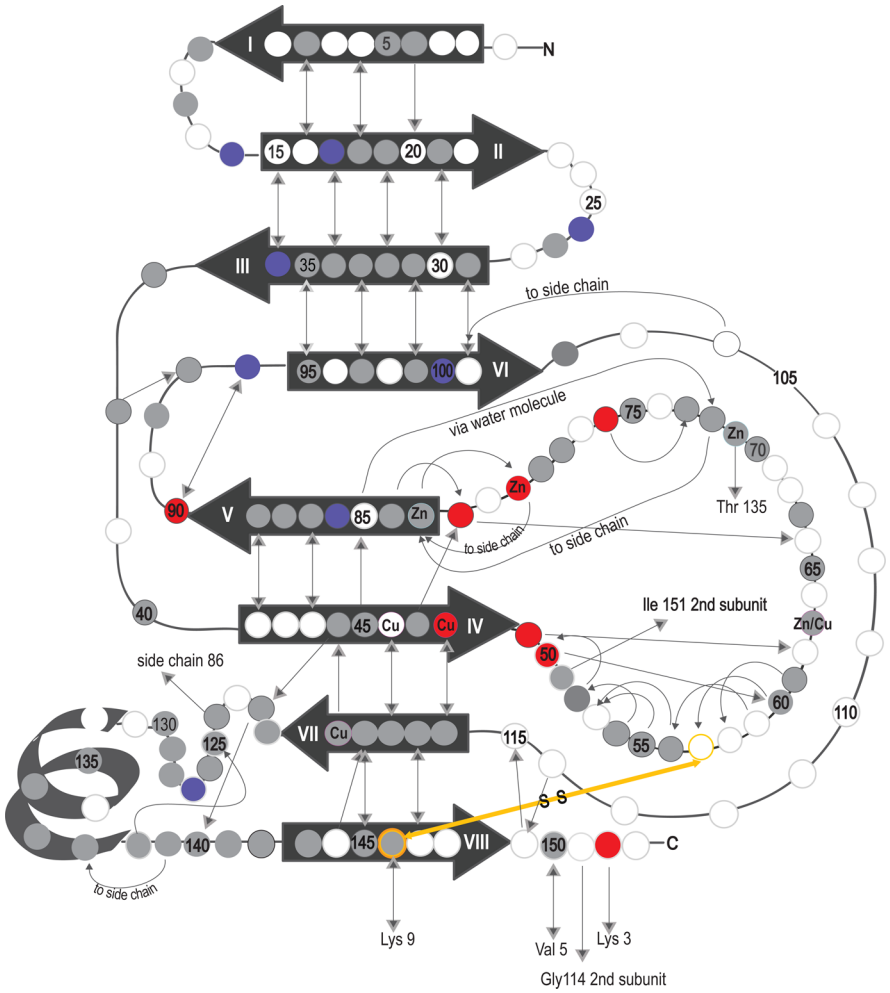

Figure 3. Schematic of one CuZnSOD subunit showing the differences in exchange patterns at 25 °C for the I113T variant compared to wild-type CuZnSOD (referring to ref 34). Amino acids that are destabilized in I113T ($\Delta G_{WT} - \Delta G_{I113T} \geq 1.5$ kcal/mol) are colored red. Amide protons that are stabilized in I113T ($\Delta G_{WT} - \Delta G_{I113T} \leq 1.5$ kcal/mol) are colored blue. Amino acids for which the H/D exchange rate was similar in wild-type CuZnSOD and I113T are colored gray. Amino acids that are not assigned (prolines included) due to overlap and weak or missing peaks are colored white. Copper and zinc binding sites are labeled with Cu and Zn, respectively. The black numbered arrows illustrate the eight β-sheets, and the gray arrows between the amino acids indicate hydrogen bonds in the secondary structure, as determined from the crystal structure (PDB accession no. 2C9V) pointing from H to O.

for several days (Figure 1). For the latter, the sample preparation took 8 min, including setup of the NMR experiment. In addition, each experiment took 30 min. Therefore, a conservative estimate of the dead time is 38 min. Thus, from the obtained exchange rates, the amino acid residues can be divided into four categories: (a) Residues with $t_{1/2}$ between 10 ms and 1 s are obtained as well-determined values (15 residues). (b) However, due to the dead time of the H/D exchange experiment, 48 residues exhibiting exchange with $t_{1/2}$ in the range between 1 s and 17 min cannot be reliably evaluated to give well-determined values. (c) The H/D exchange experiment yielded well-determined values for 30 residues having $t_{1/2}$ between 17 min and 13 days, i.e., the intensity decay was observable, and exponential fitting was possible. (d) For 32 residues, the intensities did not decay at all during the experiment and therefore these residues have $t_{1/2}$ longer than 13 days. All values are listed in Supporting Information Table S1 and visualized schematically in Figure 2. Amide protons having fast exchange with $t_{1/2}$ between 10 ms and 1 s are almost exclusively found in loops and highly surface-exposed regions. Most notably, at least 22 residues out of 34 in the metal binding loop have rapid amide proton exchange with $t_{1/2}$ between 10 ms and 17 min, i.e., most of the metal binding loop is highly dynamical in I113T under these near physiological conditions at 37 °C.

H/D and Water Exchange in the I113T Variant at 25 °C. The amide proton exchange properties of the I113T variant were also determined at 25 °C for two reasons: first, to investigate whether there are any regions in I113T where the amide proton exchange rates increase abnormally between 25 and 37 °C, i.e., to find putative regions with highly temperature-sensitive dynamics. Second, the experiment at 25 °C makes it possible to compare these results with those from similar experiments that have been conducted on the wild-type protein and on the G93A variant at 25 °C. Here, the length of the H/D exchange experiment was reduced to 3.5 days, and time points were taken only every 1.5 h. Nevertheless, reliable values were obtained for the same residues as at 37 °C (see Supporting Information Table S2 and Figure S1).

When the results for I113T at the two temperatures are compared, one can note that for the majority of the residues the exchange rates increase by approximately 1 order of magnitude

DOI: 10.1021/bi500606j
Biochemistry 2015, 54, 323−333

upon raising the temperature to 37 °C. Interestingly, two regions in the protein stand out as exceptional because they each contain clusters of three neighboring amino acid residues in which the exchange rates increase by more than 3 orders of magnitude upon increasing the temperature from 25 to 37 °C. These regions are the β-strand I (residues Ala4, Cys6, and Lys9) and three residues in the metal binding loop (residues Gly51, Asn53, and Thr54). Notably, the neighboring residues His48, Glu49, Phe50, Ala55, and Gly56 all have high exchange rates at both temperatures. Taken together, these results show that the residues 48−51 and 53−56 are highly dynamical at 37 °C and indicate that the dynamics at these residues might affect the dynamics at β-strand I.

Differences and Similarities between the Wild-Type Protein and the ALS-Associated Variants G93A and I113T. A schematic comparison of exchange rates between wild-type CuZnSOD and the I113T variant at 25 °C is shown in Figure 3. As in the wild-type protein, the interactions among β-strands I, II, III, IV, V, VII, and VIII are very stable also in G93A and I113T, and the amide protons exchange very slowly. The stable hydrogen-bond network among β-strand I, β-strand VIII, and the C-terminal part, as reported for the wild-type protein and the G93A mutant, is also stable in the mutant I113T. For example, the interaction between Val5 and Gly150 seems to be intact still, as shown by the half-life of 7 days for Val5 and Gly150. The first part of loop 7, called the electrostatic loop, is rather stable in I113T with intact hydrogen bonding (121−142, 122−140, 124−86 side chain, 125−138, and 126−124). The remaining part and the following α-helix are in very fast exchange. Thus, loop 7 and the helical part have very similar properties as those of the wild-type protein. The local breathing dynamics for the hydrogen-bonded Val17 in β-strand II to Ser34 in β-strand III is slightly stabilized in I113T, as in the G93A mutant,[34] when compared to that in the wild-type protein. Notably, the I113T mutation results in a stabilization at six positions (14, 17, 26, 36, 37, and 100) in or close to the connected β-strands II, III, and VI when compared to the wild-type protein.

The most pronounced destabilizing effects of the I113T and G93A mutations are found in the metal binding loop and at positions neighboring this loop. In I113T, the copper ligand His48 is destabilized by at least 2.9 kcal/mol, and Glu49 and Phe50 are destabilized by more than 9 and 8 kcal/mol, respectively. In the G93A variant, Glu49 and Phe50 are destabilized by 2.8 and 2.7 kcal/mol. The last part of the MTB-loop encloses two of the four zinc ligands. While the ligand His71 exchanges rather slowly as in the wild-type protein, His80 exchanges much faster and is destabilized by 3.7 kcal/mol in G93A and at least 7.5 kcal/mol in I113T. Also, residue Asp76, which exchanges very slowly in the wild-type protein, is destabilized in the G93A and I113T variants of this study (by 1.3 and 4 kcal/mol, respectively). The residue Gly82 is destabilized by at least 4 kcal/mol in I113T. The observed low stability in major parts of the metal binding loop seems to be coupled to neighboring parts in the structure, i.e., Ala152, which has a hydrogen bond to Lys3 in β-strand I, is destabilized by more than 2.8 kcal/mol in the I113T variant.

DISCUSSION

In this study, we set out to investigate a possible common theme of destabilization in various CuZnSOD variants. From earlier studies by Lindberg et al.,[20] it is known that the fully metal-loaded wtSOD and G93A variants have a high global stability with a midpoint (MP) for GuHCl-induced unfolding of 3.9 and 3.4 M, respectively. In the present study, we have, by using their experimental conditions, found that the I113T variant also has a very high global stability (MP = 3.9 M).

Prior to detailed residuewise analysis of exchange properties, the structural integrity of the I113T variant and its dimerization properties had to be verified. To this end, we used ^{15}N relaxation NMR experiments to estimate whether this variant tumbles as a dimer, monomer, or higher order complex in solution. The results clearly show a similar behavior between wild-type and G93A CuZnSOD, i.e., that they are stable dimers. Therefore, the hydrogen exchange experiment can be compared among these three variants. Notably, no residues exhibit conformational exchange on the millisecond time scale, confirming its very high conformational stability.[20,34] Variant I113T studied here also shows a highly stable core, since 32 residues exhibit no observable exchange at 37 °C and pH 7. Although residue 113 is close to its counterpart in the other subunit, no real contacts are established in the structure of wild-type protein. However, Thr113 and neighboring residues do not produce any observable signals in NMR experiments. This lack of signals was also observed in a previous study of the wild-type protein and G93A, where almost all signals from residues in loop 6 are broadened beyond detection.[34] It has been shown that the major structural effect of the I113T mutation is loss of the close hydrophobic contact between the methyl group of Ile113 and the Cβ of Ala4.[50] This is manifested in our study by the fast exchange of Ala4. However, we do not observe an immediate effect on dimerization.

A common theme, concerning variants I113T and G93A, however, is the destabilization of the remotely positioned MTB-loop. Metal ligands and surrounding residues in the I113T variant are even more destabilized than was observed in the G93A variant.[34] As a consequence of the destabilization caused by the I113T mutation, essentially the entire metal binding loop (MTB) has low stability. This is depicted by the observed fast exchange rates in four long stretches of the loop: residues 48−51 (HEFG), 53−56 (NTAG), 61−70 (GPHFNPLSRK), and 77−82 (EERHVG). For the N- and C-terminal parts of this loop, the destabilization is large in the G93A variant (the destabilization for Glu49, Phe50, Asp76, and His80 is >2.8, 2.7, >2.7, and >4.8 kcal/mol, respectively) and very large in the I113T variant (the destabilization for Glu49, Phe50, Asp76, His80, and Gly82 is >9.2, 8.2, >4.0, >8.5, and >4.1 kcal/mol, respectively). The center of the MTB-loop is fixed in position by the disulfide bridge between Cys57 and Cys146 of β-strand VIII. The flanking residues, in general, have rather low stability, but the terminal residues and metal binding residues are extremely destabilized in G93A and I113T. In the G93A variant, the metal binding (MTB) loop is also the most destabilized part of CuZnSOD. The lower stability and higher mobility of these residues possibly lead to local unfolding of the loop, which would expose aggregation-prone surfaces. The destabilization of the loop may partly be cooperative because several of the residues in the loop are destabilized from differing high stabilities to rather similar and low stabilities. Thus, it is possible that the destabilization of the metal binding loop is a key factor and a frequent theme of how toxicity develops in ALS-related CuZnSOD mutants. It is striking that two mutations quite distant from each other in sequence and structure (28.5 Å from NH to NH) have a very similar effect on a third region that is also rather remote from the mutation sites (10 and 14.2 Å from Thr113 to Phe50 and His80, respectively,

DOI: 10.1021/bi500606j
Biochemistry 2015, 54, 323−333

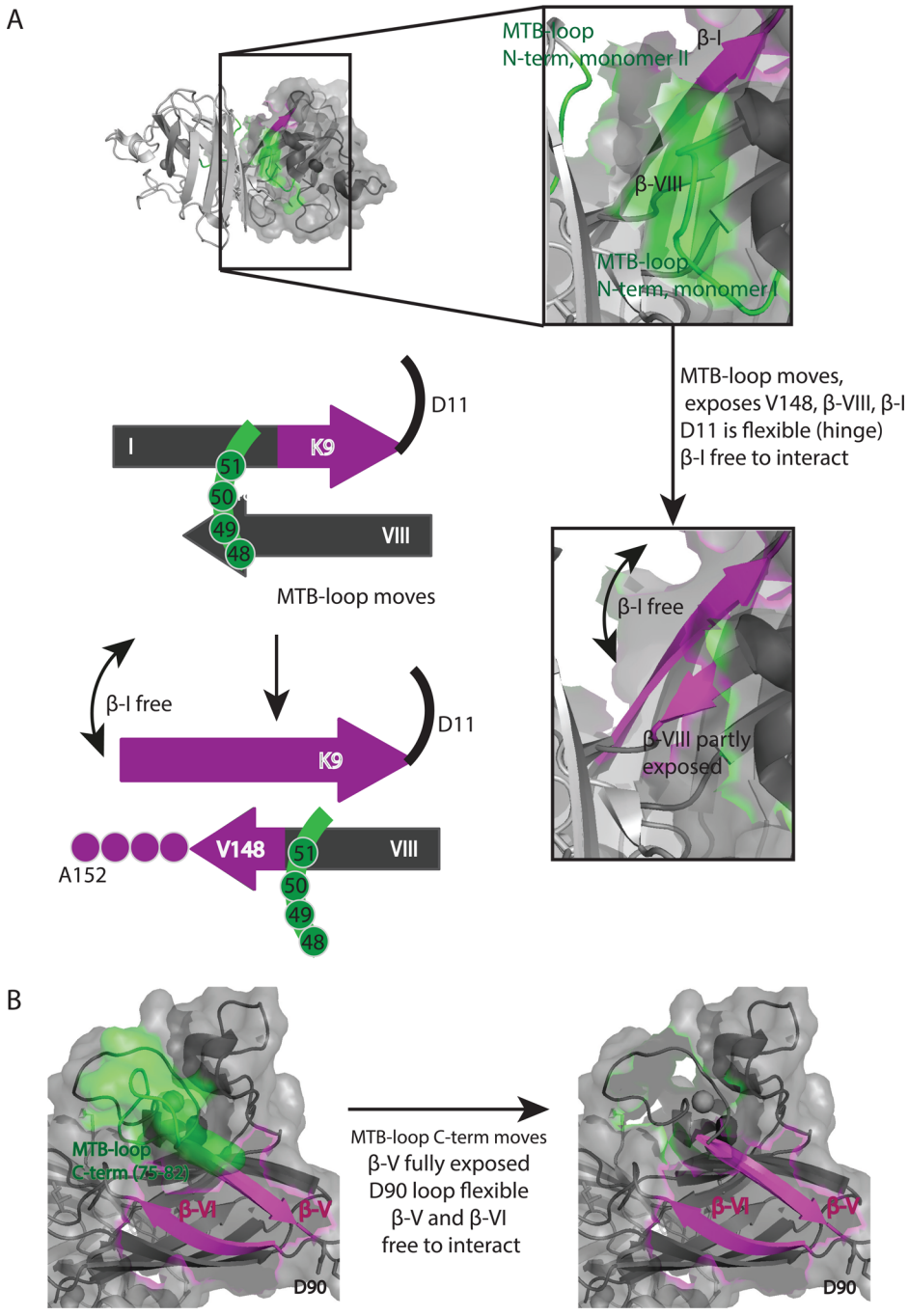

Figure 4. (A) Illustration of the first effect that opening the N-terminal part of the metal binding loop (MTB-loop, green) might have. On the left, the dimer of CuZnSOD is shown in gray. The zoomed-in region at the MTB-loop shows that, when it moves away, part of β-strand VIII is exposed, which destabilizes V148 and A152, where amide hydrogens show rather fast exchange. The extremely destabilized loop between β-strand I and II (e.g., D11) would make accessibility of β-strand I (purple) possible and could lead to new interactions. (B) The second effect of the destabilized MTB-loop (green) results from moving of its C-terminal region, exposing β-strand V. The additional destabilization of the loop (e.g., D90) connecting the already distant β-strand V and β-strand VI (purple) enables further moving of these strands and provides more interaction surface for possible aggregation.

and 28.3 and 28.2 Å from Ala93 to Phe50 and His80, respectively).

We are well-aware of a prevalent hypothesis that ALS may be caused by aggregation of metal-depleted and monomeric apo-enzymes having low stability.[18−20,31,50,57,60] Many of these studies have shown that the apo-enzymes are prone to form aggregates. However, to our knowledge, very little is known about the prevalence of monomeric apo-enzymes in cells with normal content of metals and Cu-chaperones. Several studies on other ALS-associated variants and engineered variants with lowered zinc binding affinities have indicated that the metal binding region is a hot spot for non-native self-association.[62−65] Therefore, we argue that alternative mechanisms for aggregation must be investigated as presented in the present study.

DOI: 10.1021/bi500606j
Biochemistry 2015, 54, 323−333

As shown previously for the G93A variant, CuZnSOD protein is not destabilized by the I113T mutation as a single cooperative unit, as is common for small globular proteins. Instead, on top of local destabilization at the mutation site, a common region distinct from the mutation site is affected. Apparently, the region around I113 is cooperatively coupled to the rather distant metal binding region and the long zinc binding loop 4. The mechanism for this coupling is not evident from the experimental results. It should also be noted that the Cu^{2+} ion has three side chain ligands situated in the β-strands IV and VII, indicating that it can be stably coordinated even if the bond to the ligand His63 in the metal binding loop is broken upon its dynamical movements.

The gain of toxicity has been linked to aggregation or fibril formation of CuZnSOD.[11−14,51] With the findings on G93A[34] and on I113T, presented here, we can now propose a model for how this aggregation may take place considering the slow time scales involved. The observed destabilization of the MTB-loop can have two major effects: (i) The N-terminal part of the MTB-loop (residues 48−51 and possibly 53−56) moves away, leading to exposure of a major part of β-strand I (Figure 4). The additional low stability of loop 1 (connecting strands I and II, including D11) allows β-strand I to move slightly. Thus, this side of the β-barrel now becomes solvent accessible, and β-strand I could accommodate new interactions with another protein moiety. β-strand I is close to the dimer interface, but it can nevertheless expose enough surface to induce oligomerization by interaction with a second SOD molecule (Figure 4). This suggestion is also supported by recent results from an all-atom Monte Carlo study of CuZnSOD by Bille et al., which indicated that β-strand I upon exposure has a high propensity to aggregate by forming a new intermolecular parallel β-structure.[52] In addition, analysis of the SOD sequence by the PASTA and Aggrescan algorithms both indicate that β-strand I has a high propensity to aggregate by formation of a extended β-sheet. (ii) Similarly, residues 61−70 (GPHFNPLSRK) and C-terminal residues 77−82 (EERHVG) of the MTB-loop can move and expose β-strand V and VI, allowing them to be free to interact with another CuZnSOD molecule (Figure 4). This could also result in aggregation via propagation of β-sheet formation. Of note, Bille et al.[52] found that β-strand VI also has a high propensity for aggregation by formation of novel β-strand interactions.

A combination of both of the described mechanisms can also be imagined. Oligomerization via β-sheet formation is typical of amyloid diseases, such as Alzheimer's, where a conformational change of monomer species enables a tight packing of extremely stable β-sheets.[53,54]

As no conformational change can be observed on faster millisecond time scales, this rearrangement and oligo/aggregate/fibril formation are an extremely slow process and presumably even further slowed by protein degradation via the ubiquitin system. This is in agreement with the late onset of ALS in affected patients and also with other late-life diseases such as Alzheimer's and other amyloid diseases.[1] In this context, it should also be noted that the observed increased dynamics at the metal binding loop strongly indicate that the Zn ion exchanges faster in the studied mutants than in the wild-type protein. Thus, the local structural integrity of these mutants may be strongly sensitive to age-related alterations in the environmental zinc concentration in the physiological setting.

The equilibrium concentrations of the open and closed (native) conformations at the metal binding region of the I113T variant can be estimated from K_d values for the [open]/[closed] equilibrium determined by our measurements (see Table S1 in Supporting Information). The cellular concentrations of CuZnSOD have been estimated to be between 1 and 2% of the total protein content in many cells. For our calculations, we conservatively chose a total cellular CuZnSOD concentration of 1000 nM, as determined by Beck et al.[55] for the cell-line U2O5. Using results for Phe50 (which is similar to many of the other residues in the MTB-loop) to represent the equilibrium distribution between the open and closed conformations at the metal binding loop, we can calculate the concentrations (in nM) of each form. The K_d value for the [open]/[closed] equilibrium at Phe50 is 0.034. Thus, we can calculate the concentrations (in nM) of the open and closed conformations from [open]/(1000 − [open]) = 0.034, which indicates that 33 nM CuZnSOD is in the open (aggregation prone) conformation under these conditions.

A possible first step in an aggregation process would be formation of tetrameric CuZnSOD from two dimeric CuZnSOD molecules by formation of new intermolecular interactions between the newly exposed β-strands. Assuming that a realistic binding constant for that interaction is 1 μM,[56] this would yield a cellular concentration of 1 nM CuZnSOD tetramer, a species that can rearrange and act as a seed for further aggregation. It has been argued along similar lines that oligomeric CuZnSOD is the toxic species, which has been shown to be formed in the metal-free state via new β-strand interactions and disulfide formation.[57,58] Indeed, it was possible to force CuZnSOD into fibrils under physiologically relevant conditions; however, it was still in its demetalated state without its stabilizing disulfide bridge.[51] Here, we devise a model for holo-SOD and reveal possible fibril formation nucleation sites.

We argue that a scenario of this type is more probable than a scenario in which the CuZnSOD dimer dissociates into monomeric apo-forms that subsequently unfold and form aggregated species, which earlier has been proposed.[59−61] A further argument for the suggested scenario is that we do not observe formation of any unfolded species during the 8 days of measurement under near physiological conditions.

CONCLUSIONS

Our studies have now identified that increased dynamics at the metal binding region is one putative origin for aggregation. We have proposed a model for how CuZnSOD variants can gain toxicity, independent of the location of mutation. This model is based on observations made in this study and a closely related study.[34] Notably, this study is the first to mimic near physiological conditions, including physiological temperature, 37 °C. Others have proposed that large initial alterations of the CuZnSOD structure, such as breakage of the dimer interface and subsequent global unfolding, are a prerequisite for formation of toxic CuZnSOD aggregates.[18−20,59−61] In this context, it is important to note that the global stabilities are high and strikingly similar for WT and the investigated variants, i.e., the midpoints for GuHCl induced unfolding are 3.9, 3.5, and 3.9 M, respectively. Thus, the results presented in this study instead indicate that, under physiological conditions, the formation of toxic aggregates can originate from a distinct and local destabilization of the metal binding loop as a first step, leading to initial formation of multimeric species originating from essentially well-folded molecules.

DOI: 10.1021/bi500606j
Biochemistry 2015, 54, 323−333

■ ASSOCIATED CONTENT

Supporting Information

Figure S1: Schematic of one CuZnSOD subunit showing the differences in exchange patterns for the I113T variant at 37 °C compared to 25 °C. Tables S1 and S2: Experimentally determined exchange values for I113T at 25 and 37 °C. This material is available free of charge via the Internet at http://pubs.acs.org.

■ AUTHOR INFORMATION

Corresponding Author

*E-mail: nalle@ifm.liu.se.

Funding

The study was supported by grants from the Swedish Research Council to B.-H.J. (Dnr 2006-4253) and P.L. (Dnr 621-2012-5136).

Notes

The authors declare no competing financial interest.

■ ACKNOWLEDGMENTS

We thank the Swedish NMR center in Gothenburg for measurement time at the 800 MHz spectrometer. J.H. gratefully acknowledges Forum Scientium for financial support, the Swedish Research Council (Vetenskapsrådet), and the European Molecular Biology Organization (EMBO, ALTF 276-2010) for postdoc fellowships.

■ ABBREVIATIONS

SOD, superoxide dismutase; ALS, amyotrophic lateral sclerosis; yCCS, yeast copper chaperone for superoxide dismutase

■ REFERENCES

(1) Soto, C. (2003) Unfolding the role of protein misfolding in neurodegenerative diseases. *Nat. Rev. Neurosci. 4*, 49−60.

(2) Orrell, R. W., Habgood, J. J., Gardiner, I., King, A. W., Bowe, F. A., Hallewell, R. A., Marklund, S. L., Greenwood, J., Lane, R. J., and deBelleroche, J. (1997) Clinical and functional investigation of 10 missense mutations and a novel frameshift insertion mutation of the gene for copper-zinc superoxide dismutase in UK families with amyotrophic lateral sclerosis. *Neurology 48*, 746−751.

(3) (1998) *Principles of Neurology* (Adams, R., Vinctor, M., and Ropper, A., Eds.) McGraw-Hill Health Professions Divisions, New York.

(4) Deng, H. X., Hentati, A., Tainer, J. A., Iqbal, Z., Cayabyab, A., Hung, W. Y., Getzoff, E. D., Hu, P., Herzfeldt, B., Roos, R. P., et al. (1993) Amyotrophic lateral sclerosis and structural defects in Cu,Zn superoxide dismutase. *Science 261*, 1047−1051.

(5) Elshafey, A., Lanyon, W. G., and Connor, J. M. (1994) Identification of a new missense point mutation in exon 4 of the Cu/Zn superoxide dismutase (SOD-1) gene in a family with amyotrophic lateral sclerosis. *Hum. Mol. Genet. 3*, 363−364.

(6) Rosen, D. R., Siddique, T., Patterson, D., Figlewicz, D. A., Sapp, P., Hentati, A., Donaldson, D., Goto, J., O'Regan, J. P., Deng, H. X., et al. (1993) Mutations in Cu/Zn superoxide dismutase gene are associated with familial amyotrophic lateral sclerosis. *Nature 362*, 59−62.

(7) Guegan, C., and Przedborski, S. (2003) Programmed cell death in amyotrophic lateral sclerosis. *J. Clin. Invest. 111*, 153−161.

(8) Borchelt, D. R., Lee, M. K., Slunt, H. S., Guarnieri, M., Xu, Z. S., Wong, P. C., Brown, R. H., Jr., Price, D. L., Sisodia, S. S., and Cleveland, D. W. (1994) Superoxide dismutase 1 with mutations linked to familial amyotrophic lateral sclerosis possesses significant activity. *Proc. Natl. Acad. Sci. U.S.A. 91*, 8292−8296.

(9) Gurney, M. E., Pu, H., Chiu, A. Y., Dal Canto, M. C., Polchow, C. Y., Alexander, D. D., Caliendo, J., Hentati, A., Kwon, Y. W., Deng, H. X., et al. (1994) Motor neuron degeneration in mice that express a human Cu,Zn superoxide dismutase mutation. *Science 264*, 1772−1775.

(10) Reaume, A. G., Elliott, J. L., Hoffman, E. K., Kowall, N. W., Ferrante, R. J., Siwek, D. F., Wilcox, H. M., Flood, D. G., Beal, M. F., Brown, R. H., Jr., Scott, R. W., and Snider, W. D. (1996) Motor neurons in Cu/Zn superoxide dismutase-deficient mice develop normally but exhibit enhanced cell death after axonal injury. *Nat. Genet. 13*, 43−47.

(11) Bruijn, L. I., Houseweart, M. K., Kato, S., Anderson, K. L., Anderson, S. D., Ohama, E., Reaume, A. G., Scott, R. W., and Cleveland, D. W. (1998) Aggregation and motor neuron toxicity of an ALS-linked SOD1 mutant independent from wild-type SOD1. *Science 281*, 1851−1854.

(12) Durham, H. D., Roy, J., Dong, L., and Figlewicz, D. A. (1997) Aggregation of mutant Cu/Zn superoxide dismutase proteins in a culture model of ALS. *J. Neuropathol. Exp. Neurol. 56*, 523−530.

(13) Johnston, J. A., Dalton, M. J., Gurney, M. E., and Kopito, R. R. (2000) Formation of high molecular weight complexes of mutant Cu,Zn-superoxide dismutase in a mouse model for familial amyotrophic lateral sclerosis. *Proc. Natl. Acad. Sci. U.S.A. 97*, 12571−12576.

(14) Rousseau, F., Schymkowitz, J., and Oliveberg, M. (2008) ALS precursor finally shaken into fibrils. *Proc. Natl. Acad. Sci. U.S.A. 105*, 18649−18650.

(15) Banci, L., Bertini, I., Cramaro, F., Del Conte, R., Rosato, A., and Viezzoli, M. S. (2000) Backbone dynamics of human Cu,Zn superoxide dismutase and of its monomeric F50E/G51E/E133Q mutant: the influence of dimerization on mobility and function. *Biochemistry 39*, 9108−9118.

(16) Hart, P. J., Liu, H., Pellegrini, M., Nersissian, A. M., Gralla, E. B., Valentine, J. S., and Eisenberg, D. (1998) Subunit asymmetry in the three-dimensional structure of a human CuZnSOD mutant found in familial amyotrophic lateral sclerosis. *Protein Sci. 7*, 545−555.

(17) Hayward, L. J., Rodriguez, J. A., Kim, J. W., Tiwari, A., Goto, J. J., Cabelli, D. E., Valentine, J. S., and Brown, R. H., Jr. (2002) Decreased metallation and activity in subsets of mutant superoxide dismutases associated with familial amyotrophic lateral sclerosis. *J. Biol. Chem. 277*, 15923−15931.

(18) Jonsson, P. A., Graffmo, K. S., Andersen, P. M., Brannstrom, T., Lindberg, M., Oliveberg, M., and Marklund, S. L. (2006) Disulphide-reduced superoxide dismutase-1 in CNS of transgenic amyotrophic lateral sclerosis models. *Brain 129*, 451−464.

(19) Lindberg, M. J., Bystrom, R., Boknas, N., Andersen, P. M., and Oliveberg, M. (2005) Systematically perturbed folding patterns of amyotrophic lateral sclerosis (ALS)-associated SOD1 mutants. *Proc. Natl. Acad. Sci. U.S.A. 102*, 9754−9759.

(20) Lindberg, M. J., Tibell, L., and Oliveberg, M. (2002) Common denominator of Cu/Zn superoxide dismutase mutants associated with amyotrophic lateral sclerosis: decreased stability of the apo state. *Proc. Natl. Acad. Sci. U.S.A. 99*, 16607−16612.

(21) Rodriguez, J. A., Valentine, J. S., Eggers, D. K., Roe, J. A., Tiwari, A., Brown, R. H., Jr., and Hayward, L. J. (2002) Familial amyotrophic lateral sclerosis-associated mutations decrease the thermal stability of distinctly metallated species of human copper/zinc superoxide dismutase. *J. Biol. Chem. 277*, 15932−15937.

(22) Fridovich, I. (1995) Superoxide radical and superoxide dismutases. *Ann. Rev. Biochem. 64*, 97−112.

(23) Pardo, C. A., Xu, Z., Borchelt, D. R., Price, D. L., Sisodia, S. S., and Cleveland, D. W. (1995) Superoxide dismutase is an abundant component in cell bodies, dendrites, and axons of motor neurons and in a subset of other neurons. *Proc. Natl. Acad. Sci. U.S.A. 92*, 954−958.

(24) Getzoff, E. D., Tainer, J. A., Weiner, P. K., Kollman, P. A., Richardson, J. S., and Richardson, D. C. (1983) Electrostatic recognition between superoxide and copper, zinc superoxide dismutase. *Nature 306*, 287−290.

(25) Parge, H. E., Hallewell, R. A., and Tainer, J. A. (1992) Atomic structures of wild-type and thermostable mutant recombinant human

DOI: 10.1021/bi500606j
Biochemistry 2015, 54, 323−333

Cu,Zn superoxide dismutase. *Proc. Natl. Acad. Sci. U.S.A. 89*, 6109−6113.
(26) Tainer, J. A., Getzoff, E. D., Richardson, J. S., and Richardson, D. C. (1983) Structure and mechanism of copper, zinc superoxide dismutase. *Nature 306*, 284−287.
(27) Hallewell, R. A., Imlay, K. C., Lee, P., Fong, N. M., Gallegos, C., Getzoff, E. D., Tainer, J. A., Cabelli, D. E., Tekamp-Olson, P., Mullenbach, G. T., et al. (1991) Thermostabilization of recombinant human and bovine CuZn superoxide dismutases by replacement of free cysteines. *Biochem. Biophys. Res. Commun. 181*, 474−480.
(28) Bartnikas, T. B., and Gitlin, J. D. (2001) How to make a metalloprotein. *Nat. Struct. Biol. 8*, 733−734.
(29) Valentine, J. S., and Gralla, E. B. (1997) Delivering copper inside yeast and human cells. *Science 278*, 817−818.
(30) Ahl, I. M., Lindberg, M. J., and Tibell, L. A. (2004) Coexpression of yeast copper chaperone (yCCS) and CuZn-superoxide dismutases in *Escherichia coli* yields protein with high copper contents. *Protein Expression Purif. 37*, 311−319.
(31) Shaw, B. F., and Valentine, J. S. (2007) How do ALS-associated mutations in superoxide dismutase 1 promote aggregation of the protein? *Trends Biochem. Sci. 32*, 78−85.
(32) Orrell, R. W., Habgood, J. J., Malaspina, A., Mitchell, J., Greenwood, J., Lane, R. J., and deBelleroche, J. S. (1999) Clinical characteristics of SOD1 gene mutations in UK families with ALS. *J. Neurol. Sci. 169*, 56−60.
(33) Mockett, R. J., Radyuk, S. N., Benes, J. J., Orr, W. C., and Sohal, R. S. (2003) Phenotypic effects of familial amyotrophic lateral sclerosis mutant SOD alleles in transgenic *Drosophila*. *Proc. Natl. Acad. Sci. U.S.A. 100*, 301−306.
(34) Museth, A. K., Brorsson, A. C., Lundqvist, M., Tibell, L. A., and Jonsson, B. H. (2009) The ALS-associated mutation G93A in human copper-zinc superoxide dismutase selectively destabilizes the remote metal binding region. *Biochemistry 48*, 8817−8829.
(35) Shipp, E. L., Cantini, F., Bertini, I., Valentine, J. S., and Banci, L. (2003) Dynamic properties of the G93A mutant of copper-zinc superoxide dismutase as detected by NMR spectroscopy: implications for the pathology of familial amyotrophic lateral sclerosis. *Biochemistry 42*, 1890−1899.
(36) Delaglio, F., Grzesiek, S., Vuister, G. W., Zhu, G., Pfeifer, J., and Bax, A. (1995) NMRPipe: a multidimensional spectral processing system based on UNIX pipes. *J. Biomol. NMR 6*, 277−293.
(37) Sattler, M., Schleucher, J., and Griesinger, C. (1999) Heteronuclear multidimensional NMR experiments for the structure determination of proteins in solution employing pulsed field gradients. *Prog. Nucl. Magn. Reson. Spectrosc. 34*, 93−158.
(38) Ahlner, A., Carlsson, M., Jonsson, B. H., and Lundstrom, P. (2013) PINT: a software for integration of peak volumes and extraction of relaxation rates. *J. Biomol. NMR 56*, 191−202.
(39) Farrow, N. A., Muhandiram, R., Singer, A. U., Pascal, S. M., Kay, C. M., Gish, G., Shoelson, S. E., Pawson, T., Forman-Kay, J. D., and Kay, L. E. (1994) Backbone dynamics of a free and phosphopeptide-complexed Src homology 2 domain studied by ^{15}N NMR relaxation. *Biochemistry 33*, 5984−6003.
(40) Korzhnev, D. M., Skrynnikov, N. R., Millet, O., Torchia, D. A., and Kay, L. E. (2002) An NMR experiment for the accurate measurement of heteronuclear spin-lock relaxation rates. *J. Am. Chem. Soc. 124*, 10743−10753.
(41) Carr, H. A., and Purcell, E. (1954) Effects of diffusion on free precession in nuclear magnetic resonance experiments. *Phys. Rev. 94*, 630−638.
(42) Meiboom, S., and Gill, D. (1958) Modified spin-echo method for measuring nuclear relaxation times. *Rev. Sci. Instrum. 29*, 688−691.
(43) Vallurupalli, P., Hansen, D. F., Stollar, E., Meirovitch, E., and Kay, L. E. (2007) Measurement of bond vector orientations in invisible excited states of proteins. *Proc. Natl. Acad. Sci. U.S.A. 104*, 18473−18477.
(44) Dosset, P., Hus, J. C., Blackledge, M., and Marion, D. (2000) Efficient analysis of macromolecular rotational diffusion from heteronuclear relaxation data. *J. Biomol. NMR 16*, 23−28.
(45) McConnell, H. M. (1958) Reaction rates by nuclear magnetic resonance. *J. Chem. Phys. 28*, 430−431.
(46) Mori, S., van Zijl, P. C., and Shortle, D. (1997) Measurement of water−amide proton exchange rates in the denatured state of staphylococcal nuclease by a magnetization transfer technique. *Proteins 28*, 325−332.
(47) Bai, Y., Milne, J. S., Mayne, L., and Englander, S. W. (1993) Primary structure effects on peptide group hydrogen exchange. *Proteins 17*, 75−86.
(48) Kay, L. E., Torchia, D. A., and Bax, A. (1989) Backbone dynamics of proteins as studied by ^{15}N inverse detected heteronuclear NMR spectroscopy: application to staphylococcal nuclease. *Biochemistry 28*, 8972−8979.
(49) Garcia de la Torre, J., Huertas, M. L., and Carrasco, B. (2000) HYDRONMR: prediction of NMR relaxation of globular proteins from atomic-level structures and hydrodynamic calculations. *J. Magn. Reson. 147*, 138−146.
(50) Hough, M. A., Grossmann, J. G., Antonyuk, S. V., Strange, R. W., Doucette, P. A., Rodriguez, J. A., Whitson, L. J., Hart, P. J., Hayward, L. J., Valentine, J. S., and Hasnain, S. S. (2004) Dimer destabilization in superoxide dismutase may result in disease-causing properties: structures of motor neuron disease mutants. *Proc. Natl. Acad. Sci. U.S.A. 101*, 5976−5981.
(51) Chattopadhyay, M., Durazo, A., Sohn, S. H., Strong, C. D., Gralla, E. B., Whitelegge, J. P., and Valentine, J. S. (2008) Initiation and elongation in fibrillation of ALS-linked superoxide dismutase. *Proc. Natl. Acad. Sci. U.S.A. 105*, 18663−18668.
(52) Bille, A., Jonsson, S. A. E., Akke, M., and Irback, A. (2013) Local unfolding and aggregation mechanisms of SOD1: a Monte Carlo exploration. *J. Phys. Chem. B 117*, 9194−9202.
(53) Nelson, R., Sawaya, M. R., Balbirnie, M., Madsen, A. O., Riekel, C., Grothe, R., and Eisenberg, D. (2005) Structure of the cross-beta spine of amyloid-like fibrils. *Nature 435*, 773−778.
(54) Carulla, N., Caddy, G. L., Hall, D. R., Zurdo, J., Gairi, M., Feliz, M., Giralt, E., Robinson, C. V., and Dobson, C. M. (2005) Molecular recycling within amyloid fibrils. *Nature 436*, 554−558.
(55) Beck, M., Schmidt, A., Malmstroem, J., Claassen, M., Ori, A., Szymborska, A., Herzog, F., Rinner, O., Ellenberg, J., and Aebersold, R. (2011) The quantitative proteome of a human cell line. *Mol. Syst. Biol. 7*, 1−8.
(56) Chou, K. C., Nemethy, G., Rumsey, S., Tuttle, R. W., and Scheraga, H. A. (1986) Interactions between two beta-sheets. Energetics of beta/beta packing in proteins. *J. Mol. Biol. 188*, 641−649.
(57) Banci, L., Bertini, I., Durazo, A., Girotto, S., Gralla, E. B., Martinelli, M., Valentine, J. S., Vieru, M., and Whitelegge, J. P. (2007) Metal-free superoxide dismutase forms soluble oligomers under physiological conditions: a possible general mechanism for familial ALS. *Proc. Natl. Acad. Sci. U.S.A. 104*, 11263−11267.
(58) Banci, L., Bertini, I., Boca, M., Girotto, S., Martinelli, M., Valentine, J. S., and Vieru, M. (2008) SOD1 and amyotrophic lateral sclerosis: mutations and oligomerization. *PLoS One 3*, e1677.
(59) Rakhit, R., Crow, J. P., Lepock, J. R., Kondejewski, L. H., Cashman, N. R., and Chakrabartty, A. (2004) Monomeric Cu,Zn-superoxide dismutase is a common misfolding intermediate in the oxidation models of sporadic and familial amyotrophic lateral sclerosis. *J. Biol. Chem. 279*, 15499−15504.
(60) Hornberg, A., Logan, D. T., Marklund, S. L., and Oliveberg, M. (2007) The coupling between disulphide status, metallation and dimer interface strength in Cu/Zn superoxide dismutase. *J. Mol. Biol. 365*, 333−342.
(61) Rumfeldt, J. A., Lepock, J. R., and Meiering, E. M. (2009) Unfolding and folding kinetics of amyotrophic lateral sclerosis-associated mutant Cu,Zn superoxide dismutases. *J. Mol. Biol. 385*, 278−298.
(62) Seetharaman, S. V., Winkler, D. D., Taylor, A. B., Cao, X., Whitson, L. J., Doucette, P. A., Valentine, J. S., Schirf, V., Demeler, B., Carroll, M. C., Culotta, V. C., and Hart, P. J. (2010) Disrupted zinc-binding sites in structures of pathogenic SOD1 variants D124V and H80R. *Biochemistry 49*, 5714−5725.

DOI: 10.1021/bi500606j
Biochemistry 2015, 54, 323−333

(63) Nordlund, A., Leinartaite, L., Saraboji, K., Aisenbrey, C., Grobner, G., Zetterstrom, P., Danielsson, J., Logan, D. T., and Oliveberg, M. (2009) Functional features cause misfolding of the ALS-provoking enzyme SOD1. *Proc. Natl. Acad. Sci. U.S.A. 106*, 9667−9672.
(64) Roberts, B. R., Tainer, J. A., Getzoff, E. D., Malencik, D. A., Anderson, S. R., Bomben, V. C., Meyers, K. R., Karplus, P. A., and Beckman, J. S. (2007) Structural characterization of zinc-deficient human superoxide dismutase and implications for ALS. *J. Mol. Biol. 373*, 877−890.
(65) Antonyuk, S., Elam, J. S., Hough, M. A., Strange, R. W., Doucette, P. A., Rodriguez, J. A., Hayward, L. J., Valentine, J. S., Hart, P. J., and Hasnain, S. S. (2005) Structural consequences of the familial amyotrophic lateral sclerosis SOD1 mutant His46Arg. *Protein Sci. 14*, 1201−1213.

DOI: 10.1021/bi500606j
Biochemistry 2015, 54, 323−333